

Radiopositive Tissue Displacement Compensation for SPECT-guided Surgery

Francisco Pinto^{1,2*}, Bernhard Fuerst^{1,2*}, Benjamin Frisch²,
and Nassir Navab^{1,2}

¹ Computer Aided Medical Procedures,
Johns Hopkins University, Baltimore, MD, USA

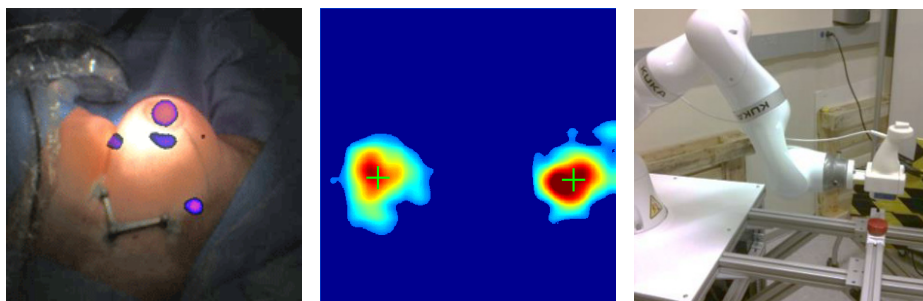
² Computer Aided Medical Procedures,
Technical University of Munich, Germany

Abstract. We present a new technique to overcome a major disadvantage of SPECT-guided surgery, where a 3D image of the distribution of a radiotracer augments the live view of the surgical situs in order to identify radiopositive tissue for resection and subsequent histological analysis. In current systems, the reconstructed SPECT volume is outdated as soon as the situs is modified by further surgical actions, due to tissue displacement. Our technique intraoperatively estimates the displacement of radiopositive tissue, which enables the update of the SPECT image augmentation. After the initial SPECT reconstruction is complete, we deploy a 2D γ -camera along with a technique to optimize its placement. We automatically establish a correspondence between regions of interest in the reconstructed volume and the near real-time 2D γ images. The 3D displacement of the radiopositive nodules is then continuously estimated based on the processing of the aforementioned γ -camera's output. Initial results show that we can estimate displacements with ± 1 mm accuracy.

1 Introduction

The Sentinel Lymph Node Biopsy (SLNB) is part of the standard of care for the treatment of melanoma [14], breast cancers [5,6] and vulvar cancers [12,15]. It further has demonstrated clinical value in the staging of head and neck [3], gastric [8], prostate [10], and cervical [4] cancers. In an SLNB, a radioactive tracer (usually a ^{99m}Tc nanocolloid) or a colored dye is injected close to a tumor, under the assumption that it primarily drains to the sentinel lymph nodes. Lymph nodes identified that way are resected and sent for subsequent histological analysis. In this paper, we focus on radioguided SLNB, which relies on either pre-interventional whole-body Single Photon Emission Computerized Tomography (SPECT) imaging or the use of a γ -detector for the live intraoperative identification of radiopositive tissue. Types of γ -detectors are 1D γ -probes and 2D γ -cameras that provide the surgeon with a planar view of the radioactivity

* F. Pinto and B. Fuerst are joint first authors.



(a) SPECT system showing several SLNs via Augmented Reality. Courtesy SurgicEye GmbH. (b) Interpolated γ -camera output for two sources, showing the auto-marked light centers. (c) γ -camera mounted on a KUKA iiwa industrial lightweight robot. An off-screen PC collects data.

Fig. 1. γ -detectors and respective outputs.

distribution in the area (see Fig. 1b). Brouwer et al. combine SPECT/CT with the intraoperative use of a laparoscopic γ -probe and γ -camera in their dual detector approach, improving SLN detection by 20% as compared to the sole use of pre-interventional information [2].

The intraoperative acquisition of several thousand γ -activity recordings over a region of interest with a spatially tracked detector allows for the 3D reconstruction of the nuclear information and its display via Augmented Reality (AR) overlays, a technique called freehand SPECT [9, 13]. The latter is applied in open and laparoscopic surgeries, such as SLNB for head and neck [7] or breast [1] cancer.

The AR visualization of SPECT information becomes outdated as soon as the tissue is manipulated, such as during any incision, when the radioactively marked tissue gets displaced. The acquisition of a new intraoperative SPECT volume to replace the previously augmented one is problematic as it requires prolonged handling of a γ -detector, delaying the procedure. Another solution is the use of a 1D or a 2D detector to acquire additional information about the γ distribution, losing the benefit of AR and disrupting the workflow. An alternate solution proposed in [11] is the registration of a pre-acquired 3D SPECT volume to an intraoperative 1D γ -probe signal, which requires a γ -probe, a model of its behavior (sensitivity, collimator aperture, etc.) and several hundred tracked γ -activity recordings. In a clinical scenario where lymph nodes can have a diameter of less than 1 cm, their demonstrated accuracy of 8 mm may prove insufficient.

Proposed Solution: Displacement Compensation. We propose a new method for continuous SLN displacement compensation. We utilize a 2D γ -camera rather than a 1D detector, and focus on minimally invasive SLN biopsies. The solution provides an update of the intraoperative SPECT image, by placing the γ -camera relative to the SLNs and estimating their displacement. Results are presented

based on displacements in ex-vivo experiments and show an average accuracy of under 1 mm.

2 Materials and Methods

The proposed displacement compensation technique requires a SPECT volume, acquired by preoperative SPECT/CT [2] or intraoperative freehand SPECT [13], and a tracked γ -camera.

2.1 SPECT Imaging and Technical Background

The system we propose is based on a two step intraoperative workflow (see Fig. 2). The first step is the acquisition of a SPECT volume. In the case of preoperative SPECT/CT, the volume has to be registered to the patient e.g. by using fiducials. In the case of freehand SPECT, registration is unnecessary as the reconstruction is done relative to an optically tracked reference target fixed to the patient's body. The SPECT volume is then visualized intraoperatively using an AR overlay, as in Fig. 1a. To display the SPECT AR overlay and its continuous updates, we employ the commercially available declipse®SPECT (SurgicEye GmbH, Munich, Bavaria, Germany). The second step is to use the tracked γ -camera to calculate the displacement of each of the segmented lymph nodes.

2.2 2D γ -camera

The CrystalCam (Crystal Photonics GmbH, Berlin, Germany) is a handheld, miniaturized γ -camera capable of producing images with a resolution of 16×16 pixels. The selected collimator, the Tungsten-based LEHS (Crystal Photonics GmbH, Berlin, Germany), has dimensions of $44 \times 44 \times 11.5$ mm, with each square pixel having 2.16 mm long sides. This is a parallel collimator; The produced images can be compared to a parallel projection of the radioactivity in the observed area. Based on a single image, a 0.925 MBq (25 Ci) ^{57}Co source is identifiable within distances up to 15 cm.

We use an infrared tracking system (henceforth designated as *IR*) to track the γ -camera and patient. The system we chose, due to the convenience of it being perfectly integrated into the declipse®SPECT system, is the Polaris Vicra (Northern Digital Inc., Waterloo, Ontario, Canada).

2.3 Displacement Compensation

Positioning of γ -camera: With the $\gamma\text{-camera}\mathbf{T}_{\text{patient}}$ transformation computed as in (1), and given that the SPECT volume is reconstructed relative to the IR patient target (in the case of freehand SPECT) or registered to the patient (in the case of preoperative SPECT/CT), we can keep the γ -camera focused on the

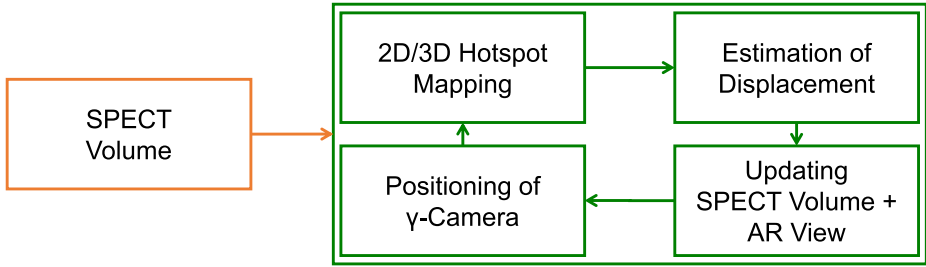


Fig. 2. The workflow of the proposed solution

global centroid of the lymph nodes. A possible robotic-assisted solution to the γ -camera positioning problem is described in Sec. 4.

$$\gamma\text{-camera}\mathbf{T}_{\text{patient}} = \gamma\text{-camera}\mathbf{T}_{\text{IR}} \cdot {}^{\text{IR}}\mathbf{T}_{\text{patient}} \quad (1)$$

2D/3D Hotspot Mapping: We segment the 3D image, via thresholding, into several ‘hotspots’ each corresponding to a different lymph node. The end objective is to translate these hotspots according to their displacement and update the AR overlay. The tissue displacement has translational and rotation components. However, since each nodule is well approximated as an anatomical structure with spherical geometry, we are interested in its 3D position. Our 2D sensor can estimate well its movement parallel to the sensor plate. We also estimate the motion orthogonal to the sensor using γ -camera’s Lookup Tables. As described within the discussion section, we also propose to guide the motion of the γ -camera based on the tracked motion of the surgical tool as the tissue displacement mostly occurs due to the tool tissue interaction. In this way, we propose a system which intelligently positions the sensor in order to dynamically optimize the estimation of radiopositive tissue displacement taking the surgical action into account.

We post process the 2D image produced by the γ -camera (see Fig. 1b for an example) by first segmenting regions of interest where the reported radioactivity is both a local and one of few global maxima. The distribution of radioactivity in the hotspot can be approximated using a Gaussian distribution. Therefore, we employ Gaussian fitting, which provides us with an estimated center for the resulting 2D blob.

Knowing both the γ -camera’s pose and the location of each lymph node computed before, we can compare the 3D SPECT hotspot centroids and 2D blob centers. This can be done by backprojecting the 3D hotspots onto the γ -camera’s collimator view plane. The same Gaussian fitting method can be applied to the backprojection and we can then establish a 3D hotspot to 2D blob mapping by comparing the distance between centers.

Estimation of Displacement: With continuous γ -camera acquisitions, we update the SPECT volume accordingly, albeit with translations solely parallel to the

γ -camera’s collimator view plane. Z -direction translations are recovered with a lesser degree of accuracy by referring to the γ -camera’s Lookup Tables (LUT), which allows the user to estimate relative, but not absolute, depth changes.

Updating SPECT Volume: After quantification of displacement is achieved as explained above, we feed back the corrections into the SPECT system, where the AR overlay (see Fig. 1a) is duly adjusted to reflect the SLNs’ translations. These are applied independently of the underlying SPECT volume’s voxel grid, thereby allowing for translations of virtually arbitrary magnitude.

3 Experiments & Results

Experimental Setup: To validate our workflow and algorithm, we perform free-hand SPECT reconstruction of a pair of sealed point-like 0.925 MBq ^{57}Co sources, which were chosen due to their similarity to ^{99m}Tc , the radioactive element usually present in the injectable nanocolloid for SPECT. ^{57}Co ’s longer half-life and safer handling makes it more suitable for laboratory use. The sources are placed on a specially designed mount so that we know their relative position with high certainty. After the reconstruction is complete, we translate the sources by several defined amounts and calculate the displacement as described in Sec. 2.3. We estimate the translations applied to each lymph node and compare them to the ground truth.

Evaluation: For our first ex-vivo experiment (Table 1), the γ -camera was kept static and placed so that the collimator’s plane was parallel to the direction of source movement. The source was moved to 5 different points ($p\{0-4\}$), which are colinear and 5 mm apart from each neighbor.

Table 1. Results for displacement estimation when $p\{0-4\}$ interdistance is 5 mm.

\hat{r}	$p1 = 5$ mm	$p2 = 10$ mm	$p3 = 15$ mm	$p4 = 20$ mm
$p0$	5.44 mm	10.92 mm	16.31 mm	21.54 mm
$p1$		5.49 mm	10.87 mm	16.11 mm
$p2$			5.39 mm	10.62 mm
$p3$				5.24 mm
$\bar{\epsilon} \approx 0.79$ mm, $\sigma \approx 0.43$ mm				

Our second ex-vivo experiment (Table 2) was done under the same circumstances, with the sole difference being that the γ -camera was angled at 45° relative to the direction of source motion.

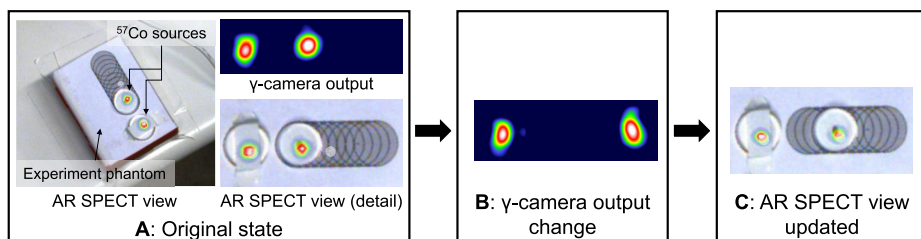


Fig. 3. Workflow for updating the SPECT AR overlay based on 2D γ -camera acquisitions. We start with original state **A**. When the tracked γ -camera's (off-screen) output changes as in **B**, the overlay is updated as in **C**.

Table 2. Results for displacement estimation when $p\{0-4\}$ interdistance is $5 \text{ mm} * \sin(45^\circ) \approx 3.54 \text{ mm}$.

\uparrow	$p1 = 3.54 \text{ mm}$	$p2 = 7.07 \text{ mm}$	$p3 = 10.61 \text{ mm}$	$p4 = 14.14 \text{ mm}$
$p0$	3.40 mm	7.06 mm	11.25 mm	14.46 mm
$p1$		3.66 mm	7.85 mm	11.07 mm
$p2$			4.19 mm	7.41 mm
$p3$				3.21 mm
$\bar{\epsilon} \approx 0.38 \text{ mm}, \sigma \approx 0.25 \text{ mm}$				

Multiple sources in view are accurately handled, as in Fig. 1b.

Performance: The algorithm operates at a frequency of 2 Hz. γ -camera output is computed using compound exposures on a sliding-window basis. The window's width is configurable and varies, but is usually between 1 to 5 seconds. Assuming 2 seconds of exposure, the end result is that displacements are presented to the user with a 2.5 second delay in the worst case, which is acceptable for an intraoperative scenario.

4 Discussion and Conclusion

Stable 2D-3D Matching: In our 2D-3D matching algorithm described in Sec. 2.3, we focus on deriving a 2D blob to 3D hotspot correspondence. This correspondence is not guaranteed to be stable in practice, i.e., a 2D blob may not always correspond to the *same* 3D hotspot. One example of this behavior occurring is if the lymph nodes move into close proximity with each other, and then apart again. However, this does not represent a major clinical problem as all radiopositive lymph nodes are treated as equivalent and the end result is their resection.

Robotic Platform for Automated Tool Tracking: Our ideal operating room setup is composed of one of the scenarios described in Sec. 2 and an additional light-weight industrial robot such as the KUKA LBR iiwa (KUKA Roboter GmbH, Augsburg, Bavaria, Germany) that would be programmed to automatically track

either the tip of a Minimally Invasive Surgery (MIS) robot's tool (as displacement is most likely to occur in its vicinity) or the centroid of the SPECT-identified lymph nodes, depending on the scenario. An example of the proposed setup is depicted in Fig. 1c.

Wide Field-of-View γ -cameras: One of the upper bounds for the quality of displacement estimation presented in this paper is the area covered by our current γ -camera. Wide field-of-view collimators would allow for improved results requiring smaller displacement of the γ -camera. Alternatively, the robotically controlled γ -camera could follow displacement of SLNs, resulting in radioguided visual servoing.

Conclusion: In this paper, we introduced a novel technique for radiopositive tissue displacement compensation. Our initial ex-vivo experiments show that estimation accuracy is in the sub-millimeter range, which motivates full integration of our approach into existing intra-operative freehand SPECT acquisition systems system and further feasibility studies.

Acknowledgements. The authors would like to thank Anton Deguet for robotics hardware support; and Intuitive Surgical Inc. for loaning the daVinci® surgical system used for testing.

References

1. Bluemel, C., Schnelzer, A., Ehlerding, A., Scheidhauer, K., Kiechle, M.: Changing the Intraoperative Nodal Status of a Breast Cancer Patient Using Freehand SPECT for Sentinel Lymph Node Biopsy. *Clinical Nuclear Medicine* 39(5), e313–e314 (2014)
2. Brouwer, O.R., Valdes Olmos, R.A., Vermeeren, L., Hoefnagel, C.A., Nieweg, O.E., Horenblas, S.: SPECT/CT and a portable gamma-camera for image-guided laparoscopic sentinel node biopsy in testicular cancer. *Journal of Nuclear Medicine* 52(4), 551–554 (2011)
3. Hellingman, D., de Wit–van der Veen, L.J., Klop, W.M.C., Olmos, R.A.V.: Detecting Near-the-Injection-Site Sentinel Nodes in Head and Neck Melanomas With a High-Resolution Portable Gamma Camera. *Clinical Nuclear Medicine* 40(1), e11–e16 (2015)
4. Holman, L.L., Levenback, C.F., Frumovitz, M.: Sentinel Lymph Node Evaluation in Women with Cervical Cancer. *Journal of Minimally Invasive Gynecology* 21(4), 540–545 (2014)
5. Krag, D.N., Anderson, S.J., Julian, T.B., Brown, A.M., Harlow, S.P., Costantino, J.P., Ashikaga, T., Weaver, D.L., Mamounas, E.P., Jalovec, L.M., Frazier, T.G., Noyes, R.D., Robidoux, A., Scarth, H.M., Wolmark, N.: Sentinel-lymph-node Resection Compared with Conventional Axillary-lymph-node Dissection in Clinically Node-negative Patients with Breast Cancer: Overall Survival Findings from the NSABP B-32 Randomised Phase 3 Trial. *The Lancet Oncology* 11(10), 927–933 (2010)

6. Lyman, G.H., Giuliano, A.E., Somerfield, M.R., Benson, A.B., Bodurka, D.C., Burstein, H.J., Cochran, A.J., Cody, H.S., Edge, S.B., Galper, S., Hayman, J.A., Kim, T.Y., Perkins, C.L., Podoloff, D.A., Sivasubramaniam, V.H., Turner, R.R., Wahl, R., Weaver, D.L., Wolff, A.C., Winer, E.P.: American Society of Clinical Oncology guideline recommendations for sentinel lymph node biopsy in early-stage breast cancer. *Journal of Clinical Oncology* 23(30), 7703–7720 (2005)
7. Mandapathil, M., Teymoortash, A., Heinis, J., Wiegand, S., Güldner, C., Hoch, S., Roefler, M., Werner, J.A.: Freehand SPECT for Sentinel Lymph Node Detection in Patients with Head and Neck Cancer: First Experiences. *Acta Oto-Laryngologica* 134(1), 100–104 (2014)
8. Miyashiro, I., Kishi, K., Yano, M., Tanaka, K., Motoori, M., Ohue, M., Ohigashi, H., Takenaka, A., Tomita, Y., Ishikawa, O.: Laparoscopic Detection of Sentinel Node in Gastric Cancer Surgery by Indocyanine Green Fluorescence Imaging. *Surgical Endoscopy* 25(5), 1672–1676 (2010)
9. Navab, N., Blum, T., Wang, L., Okur, A., Wendler, T.: First deployments of augmented reality in operating rooms. *Computer* 99, 48–55 (2012)
10. Vermeeren, L., Olmos, R.A.V., Meinhardt, W., Bex, A., van der Poel, H.G., Vogel, W.V., Sivo, F., Hoefnagel, C.A., Horenblas, S.: Value of SPECT/CT for Detection and Anatomic Localization of Sentinel Lymph Nodes Before Laparoscopic Sentinel Node Lymphadenectomy in Prostate Carcinoma. *Journal of Nuclear Medicine* 50(6), 865–870 (2009)
11. Vetter, C., Lasser, T., Okur, A., Navab, N.: 1D-3D Registration for Intra-Operative Nuclear Imaging in Radio-Guided Surgery. *IEEE Transactions on Medical Imaging* 34(2), 608–617 (2015)
12. Vidal-Sicart, S., Doménech, B., Luján, B., Pahisa, J., Torné, A., Martínez-Román, S., Lejárcegui, J.A., Fusté, P., Ordi, J., Paredes, P., Pons, F.: Sentinel Node in Gynaecological Cancers. Our Experience. *Revista Española de Medicina Nuclear (English Edition)* 28(5), 221–228 (2009)
13. Wendler, T., Hartl, A., Lasser, T., Traub, J., Daghighian, F., Ziegler, S.I., Navab, N.: Towards Intra-operative 3D Nuclear Imaging: Reconstruction of 3D Radioactive Distributions Using Tracked Gamma Probes. In: Ayache, N., Ourselin, S., Maeder, A. (eds.) MICCAI 2007, Part II. LNCS, vol. 4792, pp. 909–917. Springer, Heidelberg (2007)
14. Wong, S.L., Balch, C.M., Hurley, P., Agarwala, S.S., Akhurst, T.J., Cochran, A., Cormier, J.N., Gorman, M., Kim, T.Y., McMasters, K.M., et al.: Sentinel lymph node biopsy for melanoma: American Society of Clinical Oncology and Society of Surgical Oncology joint clinical practice guideline. *Journal of Clinical Oncology* 30(23), 2912–2918 (2012)
15. Van der Zee, A.G., Oonk, M.H., De Hullu, J.A., Ansink, A.C., Vergote, I., Verheijen, R.H., Maggioni, A., Gaarenstroom, K.N., Baldwin, P.J., Van Dorst, E.B., Van der Velden, J., Hermans, R.H., van der Putten, H., Drouin, P., Schneider, A., Sluiter, W.J.: Sentinel node dissection is safe in the treatment of early-stage vulvar cancer. *Journal of Clinical Oncology* 26(6), 884–889 (2008)